Synergistic-effect of iron-filing and silica-fume on the absorption and shrinkage of cement paste

M.O. Yusuf*
University of Hafr Al Batin, Hafr Al Batin, Saudi Arabia
* E–mail: moruf@uhb.edu.sa

Keywords: iron-filing, silica fume, water absorption, shrinkage, workability, paste

Abstract. This study investigated workability, water absorption, and drying shrinkage performances of the synergy of iron filing (IF) with silica fume (SF) in the ordinary Portland (OPC) cement paste. IF varied from 0 to 15wt. % while SF was kept constant at 10wt % of the binder. The finding revealed that at low water/binder (w/b) ratio of 0.25, the synergistic effects of the combination of IF and SF reduced the workability and shrinkage of the paste exponentially but increased water absorption. Besides, an increase in absorption was due to non-absorbent nature of IF and proliferation of interfacial transition zones (ITZ) within the matrix while addition of SF caused the increase in pore tortuosity through secondary pozzolanic reaction accompanied by its micro-filling effects. Moreover, bond characterization showed that drying shrinkage reduction was due to IF retention of evaporable water within the matrix, and the removal of hydroxyl precipitated together with an improved polymerized units of silicate. Scanning electron micrograph indicated the improvement in the microstructural density due to the formation of CASH or CSH and restriction of internal strain deformation due to the formation of Fe-infused product (CAFSH). The least shrinkage value was observed at the IF substitution level of 15% with the SF of 10%. Therefore, synergistic effects of SF and IF could enhance production of more durable concrete more especially in the hot weather climate.

1. Introduction

Iron-filings (IF) are mostly a waste product obtained from metal cutting, grinding, filing, or milling of finished iron products especially in workshops and foundry [1]. This waste (iron filing) in addition to blast furnace slag is attached to chain of iron utilization as a product or dominant component of steel alloy. There have been some studies on the uses of IF as an additive or partial supplement for sand in paste, mortar or concrete products [2]. Alserai et al. [1] conducted research on the contribution of iron filing (IF) when used together with recycled aggregates and reported its contribution to concrete mechanical properties. Alzaed [2] also reported that up to 10 % of IF could be used to improve the concrete strength while Familusi et al. [3] stated that quarry-dust used in binary could produce a concrete of better strength especially when the constituent waste materials utilized are not in excess 50 % of the total mixture.

Moreover, the increase in strength of concrete when IF is utilized has been adduced to pore blockage that enhanced reduction in porosity [4]. Olutoge et al. [5] also asserted that 20 % sand replacement could bring about 13.5 % gain in strength, and this is in consonance with the finding published by Ghannam et al. [6]. Noori and Ibrahim [7] reported a slight variation of 12 %. However, Vasudevan [8] observed decreasing in slump value and the strength with addition 5 % of IF. The difference in the percentage reported could be due to oxide composition together with impurities as many of the authors could not present the x-ray florescence (XRF) of the IF used.

Furthermore, there are several studies on shrinkage characteristics of OPC paste. For instance, Ahmad et al. [9] identified water/binder ratio as the most important factors controlling the shrinkage OPC based binder. This is followed by cement content and the presence of pozzolanic materials such as silica fume and fly-ash

contents among other factors. Bagheri et al. [10] used the silica fume in ternary blending with blast furnace slag to improve the mechanical and durability of concrete by reducing the permeability and increasing the compressive strength of the binder. Almusallam et al. [11] identified that, in the hot climate, lean-stiff concrete has higher resistance to plastic shrinkage compare to rich concrete due to the presence of more cement in the latter. The rate of evaporation and bleeding could be reduced in the concrete that contains silica fume even at the expense of the workability of the mixture. In the same manner with silica fume, Brooks and Megat Johari [12] and Guneiyisi et al. [13] pointed to the fact that inclusion of metakaolin – due to its pozzolanicity and ability to proceed on secondary hydrations – could also reduce creep, autogenous and drying shrinkage.

It has been reported that carbonation of paste and pore diameter could contribute to larger autogenous shrinkage than moisture content in alkali activated slag [14]. This is possible due to large proportion of pore sizes and radius within the slag mesoporous region [15]. Jankovic [16] used environmental scanning electron microscope (ESEM) to study interfacial transition zone (ITZ) of cement paste with a view to determining the shrinkage strain and its non-linearity with relative humidity. He concluded that type of cement, admixture and water-cement (w/c) ratio could affect the shrinkage of cement paste while wet condition of the sample could cause capillary mechanism to have significant impact. The amount of cement in the mixture could also influence the chemical and drying shrinkage in the resulting concrete. This is highlighted in the analysis of high performance concrete (HPC) used in Iowa bridge construction [17].

Moreover, Jin et al. [18] investigated the reduction of the shrinkage of AAS by using MgO and concluded that the level of reactivity of MgO together with curing condition could influence how the strength and shrinkage characteristics of alkaline activated slag (AAS) could be described. Heat-curing together with silica modulus (SiO_2/Na_2O) after 7-day of pre-curing was reported to be more effective in reducing drying shrinkage in geopolymer binder [19, 20]. The depth of the drying surface could also affect the internal drying shrinkage of concrete [21]. Slowik et al. [22] emphasized that shrinkage in plastic state of wet mortar or concrete could affect the durability performance of concrete in its hardened state. Tam et. al [23] stated that water to binder ratio could also have significant effects on the shrinkage and permeability of concrete. The use of palm oil fuel ash (POFA) up to 30 % as an additive was reported to reduce the drying shrinkage of concrete due to its high silica content that led to lower permeability of the product [24].

Meanwhile, despite these studies, no studies have addressed the water absorption, and shrinkage performance of addition of IF and SF into ordinary Portland cement paste sample with a view to understanding the bond characteristics, interaction within the microstructure, absorption and the shrinkage characteristic of the resultant product. The benefit of this study is to improve the durability characteristics (shrinkage) of concrete, promote waste valorization through utilization of more industrial waste products such as iron-filing, and to reduce the cost of green concrete production (by minimizing OPC content) which favours environmental sustainability.

2. Materials and Methods

2.1. Materials

2.1.1. Ordinary Portland cement

The cement used in the study satisfies the requirement of ASTMC 150 [25]. The oxide compositions were determined by X-ray florescence (XRF) technique and the results are as shown in Table 1 while the particle size distribution is as shown in Figure 1.

Table 1. Oxides composition of Ordinary Portland and Iron filling Oxides.

Oxides	OPC, %	Iron filing, %	Silica Fume, %
SiO_2	19.01	1.38	95.85
Al_2O_3	4.68	0.61	0.26
Fe_2O_3	3.20	96.5	0.05
CaO	66.89	0.02	0.21
MgO	0.81	–	0.45
Na_2O	0.09	–	–
TiO_2	0.22	0.03	–
K_2O	1.17	0.13	–
P_2O_5	0.08	0.05	–
SO_3	3.66	0.23	1.00
MnO	0.19	0.5	–
Cl	–	0.05	–
Cr_2O_3	–	0.11	–
ZnO	–	0.07	–
SnO	–	0.08	–
$SrO2$	–	0.02	–
CuO	–	0.22	–
LOI	2.48	–	2.80
$SiO_2 + Al_2O_3 + Fe_2O_3$	26.89	98.49	96.16
Moisture content	–	–	0.85

Юсуф М.О.
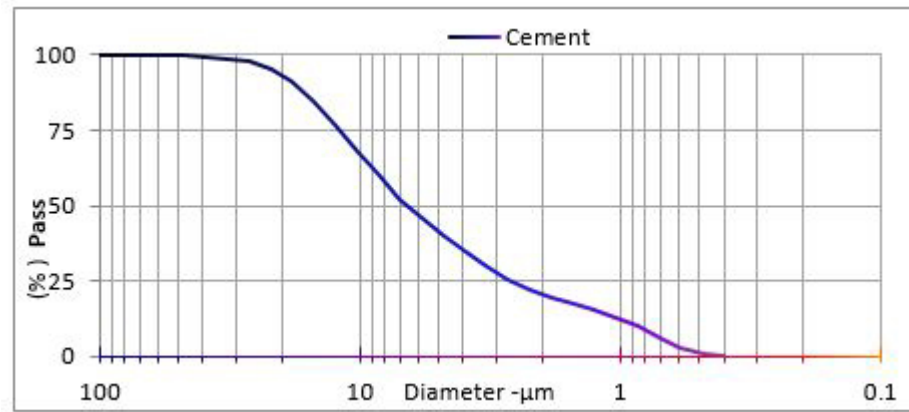
Figure 1. Particle size distribution of the ordinary Portland cement.

2.1.2. Fine aggregate

It consists of dune sand with fineness modulus of 1.85. The specific gravity in saturated dry condition was 2.62 with the absorption capacity of 0.65 %.

2.1.3. Iron-filing

The material is collected at mechanical lathe machine and brake disc grinding workshops at Senaiya Hafr Al Batin in the Eastern province of Saudi Arabia. It has the fineness modulus of 2.89 while its particle size distribution is shown in Figure 2. Its oxide composition shown in Table 1 reflects the dominance of iron oxide. The physical properties of OPC, IF powder and fine aggregates are as shown in Table 2.

Table 2. Physical properties of fine aggregates and iron filing.

Physical Properties	Sand	Iron Filing	OPC	Silica fume
Bulk Density (kg/m^3)	1699	1932	3100	630
Specific gravity	2.67	6.85	3.41	2.25
Specific surface area (m^2/kg)		13.73	331.0	18000
Fineness modulus	3.3	2.89	2.84	–
Average diameter, D50 (µm)	–	250	6.69	0.15
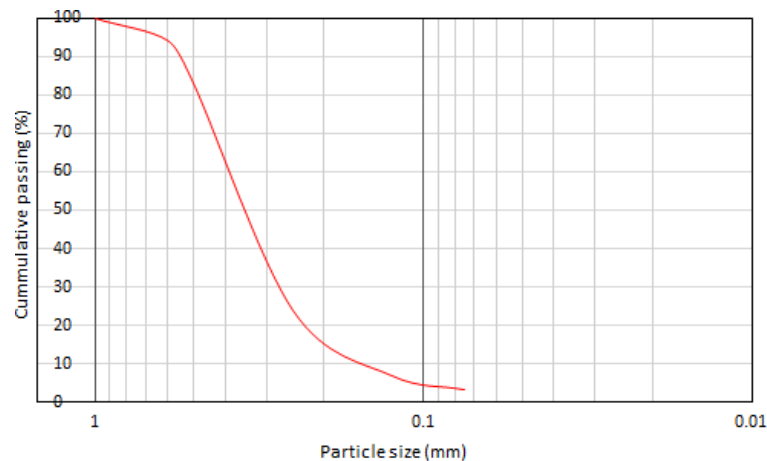
Figure 2. Particle size distribution curve of iron-filing powder.

2.1.4. Silica fume

This is a densified silica fume (SF) produced by Xiamen All Carbon Corporation, Xiamen, China and supplied by Al-Rashed Cement Co, Saudi Arabia. The material has the specific surface area of 18000 m^2/kg, and bulk density of 630 kg/m^3. Other materials physical properties are shown in Table 2 while its oxide compositions are also shown in Table 1.

2.2. Research Methodology

Mix design was conducted such that the percentage composition of the IF and SF in paste varied as 5, 10 and 15 % with addition of 10wt. % SF in all the mixtures while the water/binder (w/b) ratio was maintained as 0.25. The workability of the mixture was determined to understand the contribution of IF and SF in synergy to the consistency of the mixture. Thereafter, the hardened paste was exposed to water to study the water

absorption and shrinkage of the products due to the synergistic-effect of IF and SF. Fourier transform infrared (FTIR) spectroscopy was used to determine the impact of SF and IF on the bond characteristics of the binders. The microstructures of the samples were also examined to study the impact or contribution of IF to the densification of the paste.

2.2.1. Microstructural and Fourier infrared spectroscopic analyses

The JEOL scanning electron microscopy coupled with energy dispersive spectroscopy (SEM + EDS) model 5800 LV, was used to test the morphology of the 28-day sample paste obtained from solid sample by first coating it with gold thin fume [26, 27]. The pulverized sample was used for the FTIR spectroscopy in order to characterize the bonds that exist between the molecular compounds. FTIR was conducted using Perking Elmer 880 spectrometer using the technique of attenuated total reflection (ATR).

2.2.2. Mix proportion

Mix design was conducted such that the percentage composition of the IF varied as 0, 5, 10 and 15 % while SF was kept constant as the 1 0 % of the binder. The mix proportion is as shown in Table 3. The superplasticizer used was Glenum® of 0.63wt % by cement mass to achieve the required consistency.

Table 3. Paste material compositions.

Sample ID	OPC (kg/m^3)	Iron filing (kg/m^3)	Water (kg/m^3)	SF (kg/m^3)	SP (kg/m^3)	Unit weight (kg/m^3)
$M_{0.35}F_0So$	**1716.0**	**0.0**	**600.6**	**0.0**	**12.0**	**2328.6**
$M_{0.35}F_0S_{10}$	**1561.6**	**0.0**	**600.6**	**154.4**	**12.0**	**2328.6**
$M_{0.35}F_{05}S_{10}$	1475.8	85.8	600.9	155.3	12.0	2329.8
$M_{0.35}F_{10}S_{10}$	1390.0	171.6	600.9	155.3	12.0	2329.8
$M_{0.35}F_{15}S_{10}$	**1304.2**	**257.4**	**600.9**	**155.3**	**12.0**	**2329.8**

2.2.3. Mixing of the specimen

OPC was first placed in Hobart planetary mixer after which the SF was added and them mixed homogenously. IF powder was then added, and mixed together for 3 mins. Water (70 %) together with superplasticizer was added and then further mixed for 2 mins. The whole mixture was mixed continuously for additional 3 mins before adding the remaining water (30 %) to ensure homogeneous mixture. The pastes were then cast into 50×50×50 mm for water absorption tests while 25×25×250 mm moulds was used for shrinkage testing. The samples were demoulded after 12 hrs and then lowered into curing tank at the room temperature of 25 ± 2 °C except for the shrinkage specimens that was kept in the oven immediately at 50 °C.

2.3. Evaluation methods

2.3.1 Workability

The workability of the specimen was determined by flow table in accordance with ASTM C 1437 [28]. The slump value was expressed as a percentage as shown in Equation (1):

$$\text{Workability or slump} = \frac{\text{Measured flow} - 100}{100} \times 100. \tag{1}$$

2.3.2. Water absorption

The cubic sample of size 50 mm of known original weight were fully immersed in water while the absorption is measured by sensitive weighing balance upon drying the surface water using dry towel to ensure surface dry condition. The results are recorded as shown in Equation (2):

$$\text{Absorption (\%)} = \frac{\text{Weigth after immersion period} - \text{Original weight}}{\text{Original weight}} \times 100. \tag{2}$$

2.3.3. Drying shrinkage

To test the performance of IF in terms of drying shrinkage performance, the prismatic paste specimens of dimension 25×25×250 mm were used in triplicate while the average results were recorded by computing Equation (3).

$$\text{Shrinkage}\,(\%) = \frac{\text{Length meaured} - 250}{250} \times 100. \tag{3}$$

3. Results and Discussions

3.1. Raw materials physical properties and material characterization

The physical properties of IF shown in Table 2 indicating that IF has a bulk density of 1932 kg/m^3 which is about 62 % of that of OPC whereas SF (630 kg/m^3) is almost twice that of OPC. The specific gravity of IF – the densest of the constitutent materials – doubled that of cement, Therefore, concrete produced with IF based paste or mortar can be used for providing adequate thrust for underground buried pipes or stabilizing the pipelines. Average size D_{50} of IF was around 250 μm which could be categorized into fine aggregates in accordance with ASTM C33 [29].

Besides, the surface area of SF was higher than that of cement and IF. It has the lowest average size diameter that is capable of enhancing adequate packing within the larger particle sizes of OPC particle and IF. This frictional effects increase with the increase in the quantity of IF thereby reducing the workability of the mixtures as shown in Figure 3. Therefore, the samples without the presence of SF had better consistency in comparison with SF-free mixture. The presence of IF and SF within the cement particle increases the interfacial transition zones (ITZ). This caused and increased the inter-particle frictional resistance thereby inducing the paste low consistency by 12.5 %, With the inclusion of 5 % -10wt. % of IF, the flowability further reduced by 24 % and 25 %, respectively. The workability of the specimens varied exponentially with the IF content as shown in Equation (4). The correlation between the experimental and predicted data is as shown in Figure 4 such that the regression coefficient is 0.9 for SF = 0.1 (10 %).

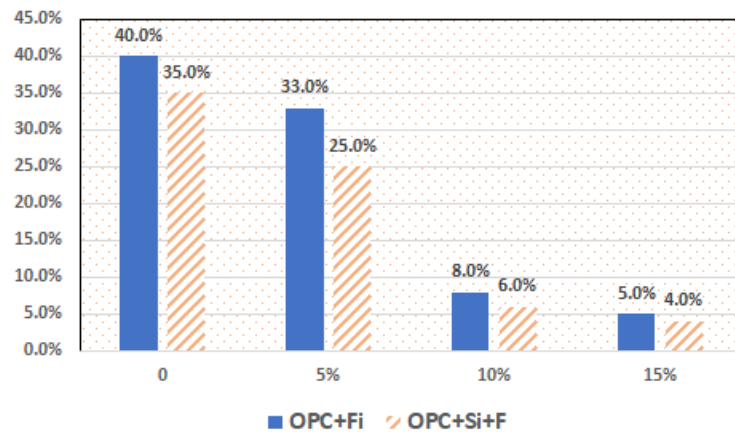$$\text{Workability} = 27.1 - 26.7e^{SF*Fe} \quad (R^2 = 0.90) \tag{4}$$

Figure 3. Workability of the paste with the presence of silica fume and iron-filing.
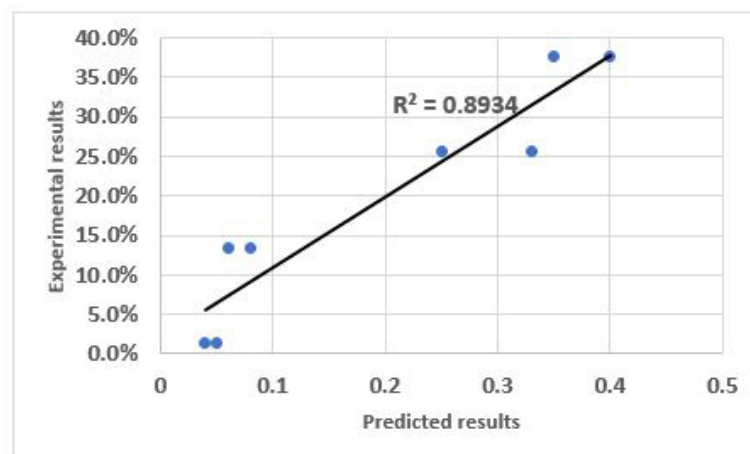

Figure 4. Workability of iron-filing and silica fume infused OPC paste.

3.2. Water absorption

Figure 5 shows percentage water absorption of paste containing iron-filing (IF). It is evident that the absorption increases with the content of IF due to its non-absorptive nature. The different between 0 and 5 % IF substitution in the absorption capacity of the sample is insignificant. However, as the increment increases

to 10 % IF, the percentage absorption increased by 36 %. The increment increases to 136.4 % as the substitution to 15 %. Presence of more IF create more ITZ thereby enhancing hydraulic permeability or conductivity of the matrix. Furthermore, the fineness of SF and its larger surface area enhance the filling of micropores thereby reducing the porosity of the matrix. This is evident in Figure 6 as the sample that contains SF within the OPC paste matrix with 5 % IF has the lower absorption in comparison with 15 % IF substitution. By comparing Figure 5 and 6, it is quite clear that SF influences the tortuosity of the microstructural pores. This is corroborated by the micrograph of SF infused sample as shown in Figure 7 and as indicated in the region 1 of the sample.

3.3. Drying shrinkage

3.3.1. Impact of iron-filing on paste shrinkage

From the specimens and their early exposure to higher temperature of 50 °C, the rate of shrinkage decreases – due to initial expansion – with increase in the content of IF in the mixture. Exposing the specimens to early heat treatment caused an abrupt reduction in the relative humidity within the matrix thereby aggravating the pore shrinkage due to surface energy change that existed between the interfaces of air/pore wall on one hand and water/pore wall on the other [30]. Further, addition of 5, 10 and 15 %wt. IF brought down the drying shrinkage value to 5.5.5, 21.1 and 23.8 %, respectively when compare to the control after 6 weeks as shown in Figure 8.
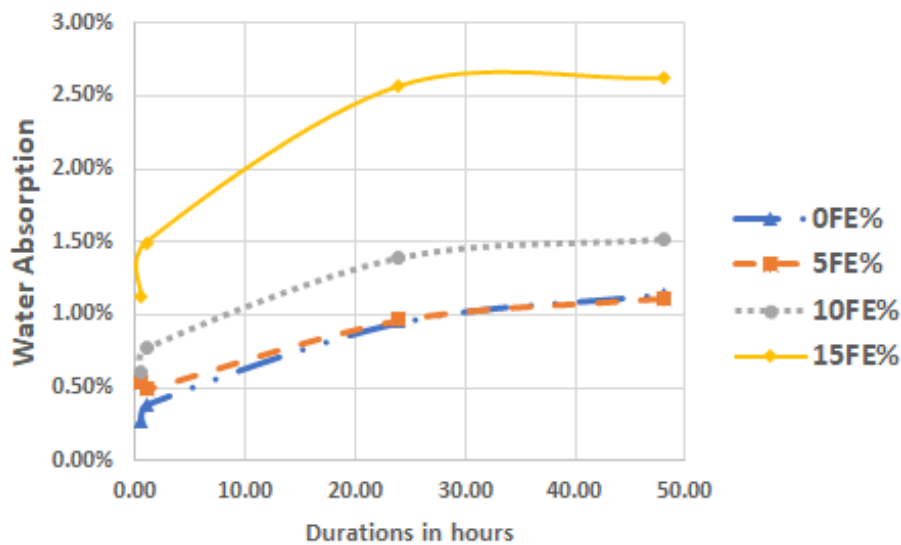

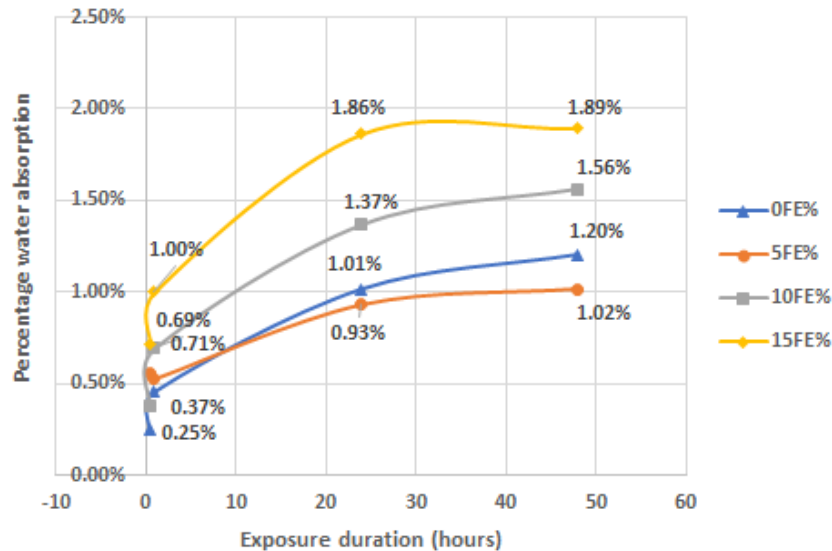**Figure 5. Water absorption based on the composition of iron-filing in paste.**

**Figure 6. Effect of varied composition of iron-filing and silica fume (10 %)
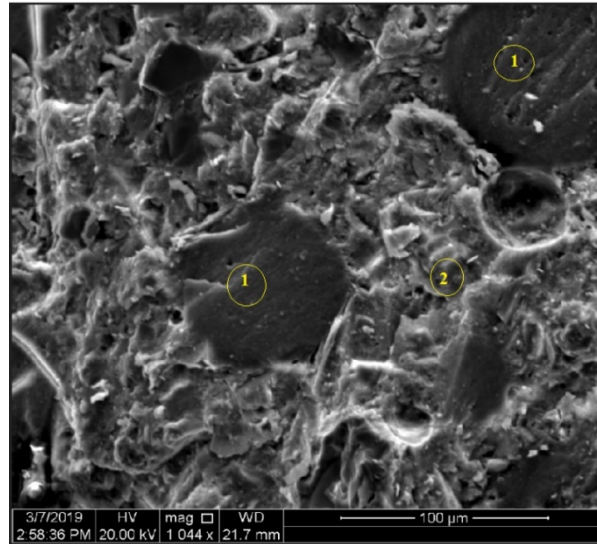on the paste water absorption.**

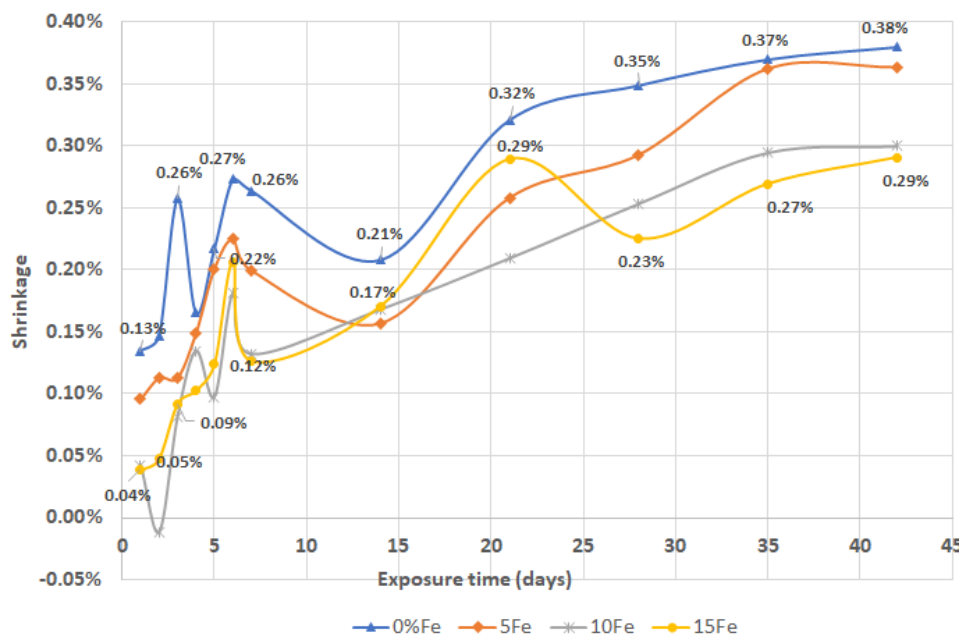**Figure 7. Micrograhs of OPC paste and silica fume.**

Figure 8. Shrinkage performance of iron-filing infused paste.

For the saturated pores, higher surface tension is developed due to the prolonged reduction in the menisci radii that accompanied dryness by ambient temperature in the oven. The aftermath of the developed surface tension due to reduction in pore relative humdity led to the development of tensile stresses within the pores and this increased with the increase in temperature in accordance with Scherer's model [31] and Kelvin's Equation (5) as reported by Adamson and Gast [32].

$$\sigma = \frac{RT}{V_m} \ln\left(\frac{RH}{X_w}\right),$$ (5)

where V_m corresponds to the pore volume;

R is the universal gas constant;

T is the temperature, RH is the relative humidity;

x_w is the mole of water per mole of pore solution that could possibly contains a solute (salts).

The developed tensile stresses had opposing effects (compression) on the pore walls thereby causing high shrinkage strains [33]. The reverse process happened during room temperature due to contraction. This induced compressive stresses caused concormitant contraction within the matrix of the microstructure. This is similar to what Sagoe-Crenstil [34] described as negative pressure within the capillary pores of the paste .The

strain curve of the control (OPC only) sample was found to be more critically wavy in the first 7 days compared to others due to absence of IF that partly absorbed the expansion and contraction by virtue of its higher conductivity (Figure 8). However, despite the alternating stresses, no visible cracks were noted on all the samples.

Moreover, the presence of IF caused restraint in internal deformation thereby leading to localized cracks or crack propagation arrest within the microstructure as shown in Figure 9. This is unlike interconnected crack in the microstructure of IF-free samples. This could be of great importance to promote utilization of IF for hot weather concreting with a view to improving the infrastructural durability challenge like shrinkage. From the FTIR spectra shown in Figure 10, it is quite evident that IF contributes to carbonation of the products by observing the deep trough of -O=C=O vibration at wavenumber 1417 cm^{-1}. It also contributes to the retention of water molecule within the matrix. This assertion stems from the observation of asymetric streching of H-O-H at the wavenumber 2985 cm^{-1} which was absent in the control sample (OPC only).
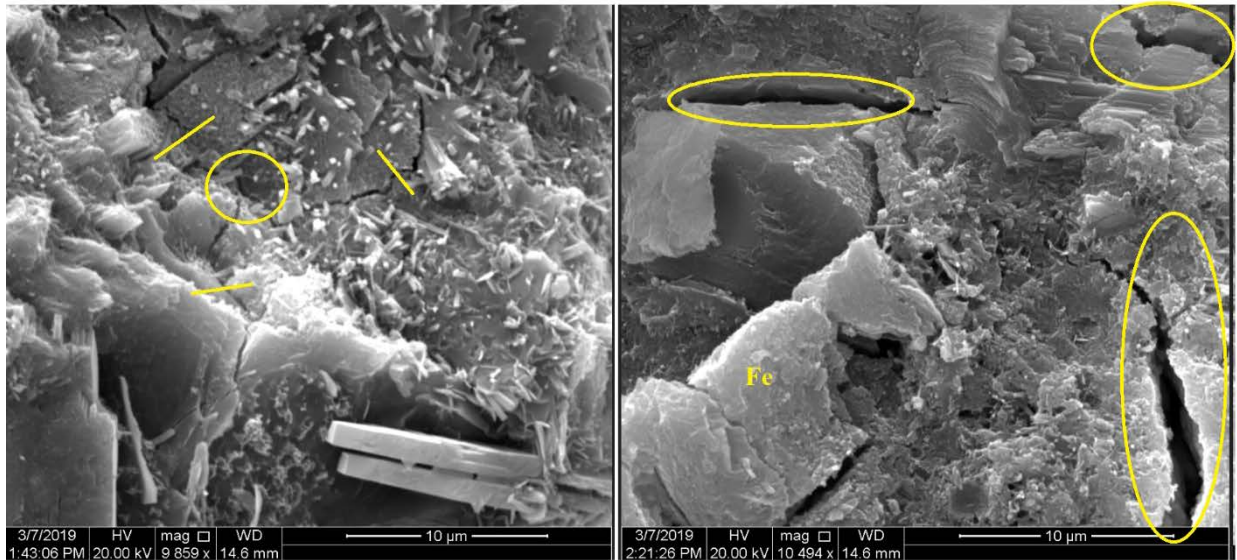

Figure 9. Micrographs of OPC paste (left) and OPC-Iron filing paste (right).
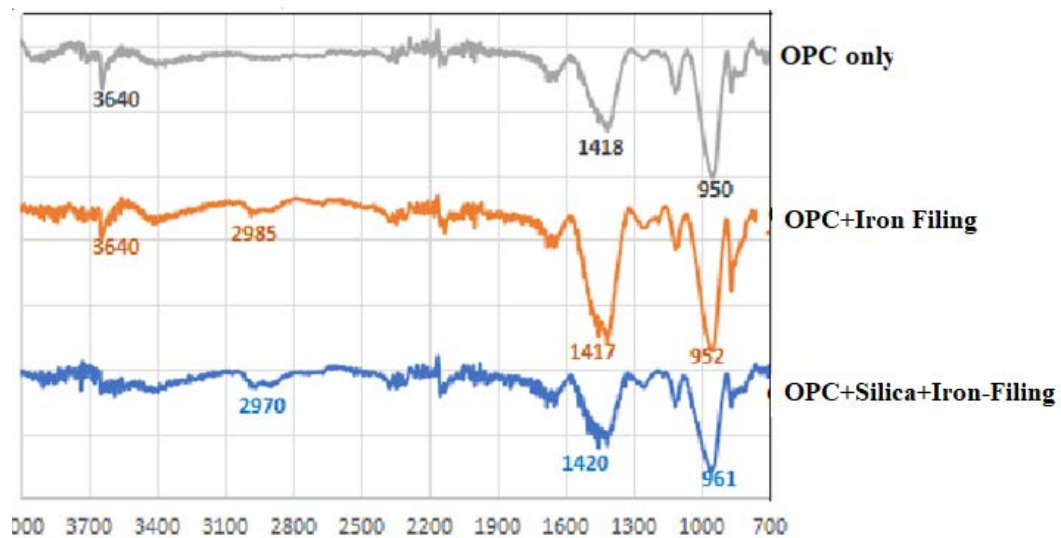

Figure 10. FTIR spectra (a) OPC only (b) OPC+10 %Fe (c) OPC+15 %Fe+10 %Si.

3.3.2. Impact of silica fume and iron-filing on shrinkage characteristics

Upon adding the silica fume (SF) into the mixture, the micro-filing effect is observed as shown in Figure 9. Figure 11 shows that the shrinkage values further reduced upon the addition of SF. For instance, the control sample is reduced by 21.1 % when comparing Figure 9 to Figure 11.
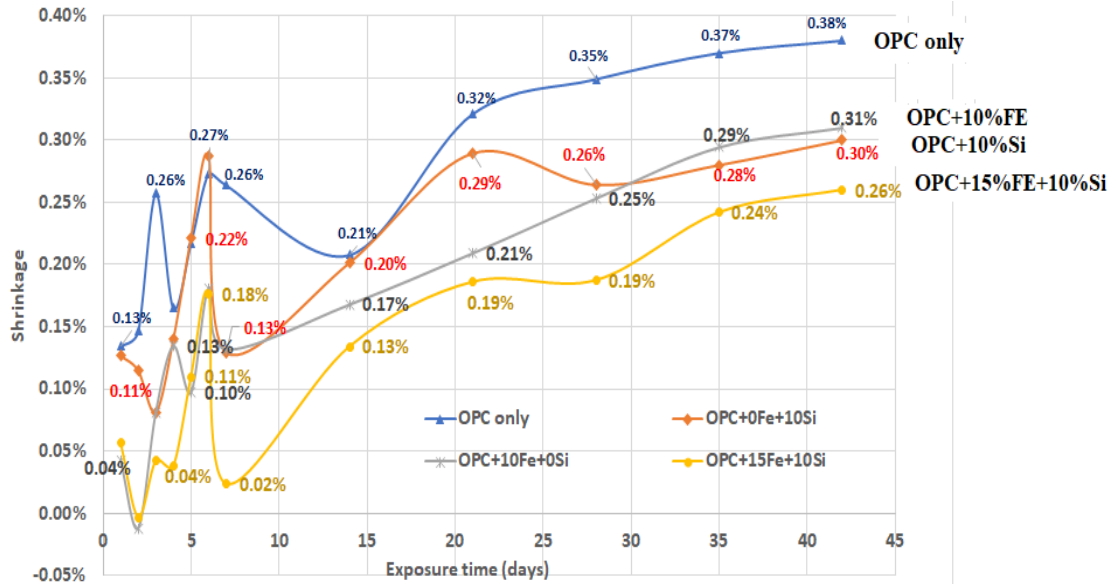
Figure 11. Impact of silica and iron-filing on the shrinkage of OPC paste.

The synergistic-effect of 15 % IF and 10 % SF reduced shrinkage further by 31.6 %. SEM+EDS shown in Figure 12 reflects the heterogeneous formations of different products within the microstructure as indicated in the regions 3, 4, 5. This suggests that the presence of the two materials enhanced pore filling and improved microstructural density as shown in regions 1 (Figures 7 and 9). Region 3 consists of Fe such that Fe/Si ratio was 0.21, while region 2 comprises more silica compare to other regions 4 and 5 (Table 4 and Figure 12).This implies that iron-filing is not uniformly distributed within the microstructure. It can be argued further that Fe present in the IF participated in the hydration process to form CA(F)SH as shown in Equation (6). This is further supported by the presence of Fe within the elements which is indicated by elemental diffractive spectroscopy (EDS) results as shown in Table 4.

$$C_3S + F + H \rightarrow CA(F)SH + CAH + CH. \tag{6}$$

The formation of calcium aluminosilicate hydrate (CASH) is also possible as shown in region 2, 4 and 5 as a result of secondary hydration or pozzolanic reactivity of SF. Further, region 5 has a low composition of alumina (Al), which implies that CSH could have probably dominated the region with traces of CASH as shown in Equation (7).

$$C_3S + CAH + S + H \rightarrow CASH + CSH + CH. \tag{7}$$
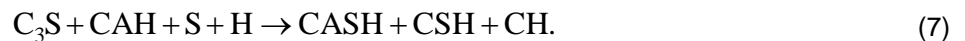
Furthermore, due to the lower water/binder (w/b=0.25) ratio, there is possibility of self dessication that mainly controls autogenous shrinkage. This phenomenon reduces the volumetric degree of saturation (S) while larger bulk density of IF (Ks) could cause decrease in the deformation as shown in Equation (8).

$$\partial = \frac{S}{3}\sigma\left(\frac{1}{K} - \frac{1}{K_s}\right), \tag{8}$$

where S is the volumetric degree of saturation and K volumetric bulk modulus of the entire mass while K_s is the volumetric modulus of solid while σ is the developed tensile stress.

4. Conclusions

The study investigated the influence of iron filing (IF) and silica fume (SF) on the paste through water absorption, shrinkage and workability of the resultant paste. This study would be of great importance to promote utilization of IF for hot weather concreting with a view to improving the infrastructural durability challenge like shrinkage. The following are the summary of the conclusions:

• The presence of IF and SF within the cement particle in the paste formation increased the interfacial transition zones that could reduce the inter-particle mobility due to frictional effect. Thus, inclusion of IF together with silica at lower water-binder ratio, and further reduced the workability of the paste.

• Water absorption value increased with the content of IF and thus 5 % IF-OPC substitution gave the better performance. It is quite clear that SF influenced the tortuosity of the microstructural pores thereby decreasing the water absorption.
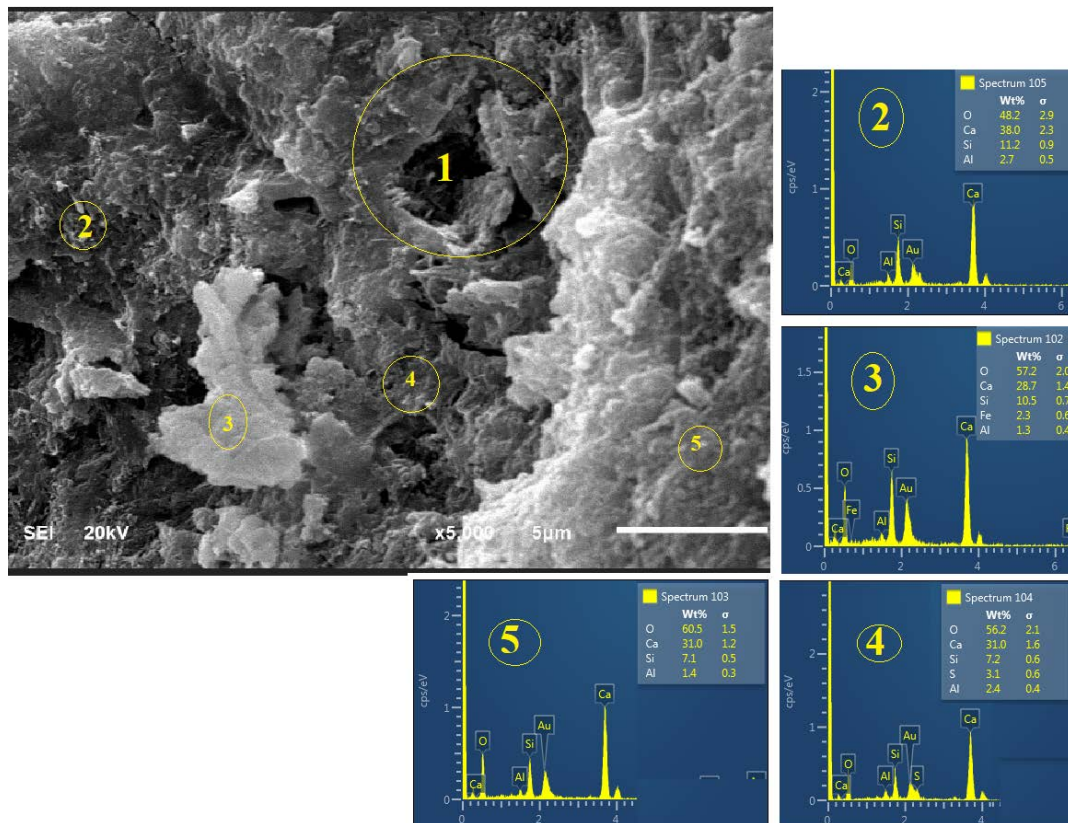
Yusuf, M.O.

Figure 12. The micrograph of 10 %Si+OPC+15 %Fe.

Table 4. Elemental ratio from EDS obtained from the micrograph.

	Region 2	Region 3	Region 4	Region 5
Ca/Si	3.6	2.75	9.9	4.32
Si/Al	0.29	8.05	3.0	5.14
Si/S	0	0	2.3	0
Fe/Si	0	0.21	0	0

- Synergy of IF and SF reduced the drying shrinkage of OPC paste as 15 % IF and 10 % SF content gave the lowest shrinkage and the better performance.

- The presence of SF at low water/binder ratio caused self-desiccation which could potentially cause autogenous shrinkage whose effect could be counter-balanced by adding IF to maintain microstructural equilibrium with consequent reduction in the resultant shrinkage.

- IF favoured the formation of H-O-H bond vibration within the matrix as SF removed the precipitate of hydroxyl through secondary hydration process as indicated by the FTIR spectra.

5. Acknowledgement

References

1. Alserai, S.J., Alsaraj, W.K., Abass Z.W. Effect of Iron Filings on the Mechanical Properties of Different Types of Sustainable Concrete. The Open Civil Engineering Journal. 2018. 12. Pp. 441–457.

2. Alzaed, A.N. Effect of Iron Filings in Concrete Compression and Tensile Strength. International Journal of Recent Development in Engineering and Technology. 2014. Vol. 3. No. 4, October.

3. Familusi, A.O., Ogundare, D.A., Adewumi, B.E., Alao, M.O. Use of quarry dust and iron filings in concrete production. 5th National Conference on Engineering Technology Held at Federal Polytechnic Offa, February, 2018.

4. Kim, J., Heo, Y., Noguchi, T. Effect of Iron Powder on Inhibition of Carbonation Process in Cementitious Materials. ISIJ International. 2015. 55(7). Pp. 1522–1530.

5. Olutoge, F.A., Onugba, M.A.O., Ocholi, A. Strength Properties of Concrete Produced With Iron Filings as Sand Replacement. British Journal of Applied Science & Technology. 2016. 18(3).

6. Ghannam, S., Najim, H., Vasconez, R. Experimental study of concrete made with granite and iron powder as partial replacement of sand. Sustainable Materials and Technology. 2016. 9. Pp. 1–9.

7. Noori, K.M.G., Ibrahim, H.H. Mechanical Properties of Concrete Using Iron Waste as a Partial Replacement of Sand. 4th International Engineering Conference on Developments in Civil & Computer Engineering, 2018. Pp. 204–215.

8. Vasudevan, G. Performance on Used Iron Sand as Concrete Admixture, 3rd International Conference on Civil. Biological and Environmental Engineering (CBEE-2016) Feb. 4–5, 2016 Bali (Indonesia), 2016. Pp. 10–13.

9. Ahmad, S., Zubair, A., Maslehuddin, M. Effect of the keymixture parameters on shrinkage of reactive powder concrete. Hindawi Publishing Corporation: Scientific World Journal. 2014. Pp. 1–8.

10. Bagheri, A.R., Zanganeh, H., Moalemi, M.M. Mechanical and durability properties of ternary concretes containing silica fume and low reactivity blast furnace slag. Cement and Concrete Compositesю 2012. 34(5). Pp. 663–670.

11. Almusallam, A.A., Maslehuddin, M., Abdul-Waris, M., Khan, M.M. Effect of mix proportions on plastic shrinkage cracking of concrete in hot environments. Construction and Building Materials Ž. 1998. 12. Pp. 353–358.

12. Brooks, J.J., Megat Johari, M.A. Effect of metakaolin on creep and shrinkage of concrete. Cement & Concrete Composites. 2001. 23. Pp. 495–502.

13. Güneyisi, E., Gesoğlu, M., Mermerdaş, K. Improving strength, drying shrinkage, and pore structure of concrete using metakaolin. Materials and Structures. 2008. 41(5). Pp. 937–949.

14. Cartwright, C., Rajabipour, F., Radlińska, A. Shrinkage Characteristics of Alkali-Activated Slag Cements, Third International Conference on Sustainable Construction Materials and Technologies, August 18 – August 21 2013, Kyoto Research Park, Kyoto, Japan, 2013. Pp. 1–9.

15. Collins, F., Sanjayan, J.G. Effect of pore size distribution on drying shrinkage of alkali-activated slag concrete. Cement and Concrete Research. 2000. 30. Pp. 1401–1406.

16. Jankovic, D. Study of 'real' shrinkage by ESEM observations and digital image analysis, repository.tudelft.nl. 2007. Pp. 1–6..

17. Wang, K., Schlorholtz, S.M., Sritharan, S., Seneviratne, H., Wang X., Hou, Q. Investigation into shrinkage of high-performance concrete used for iowa bridge decks and overlays, Paper 22. Trans Project Reports. 2013. Pp. 1–141.

18. Jin, F., Gu, K., Al-Tabbaa, A. Strength and drying shrinkage of reactive MgO modified alkali-activated slag paste. Construction and Building Materials. 2014. 51. Pp. 395–404.

19. Kani, E.N., Allahverdi, A. Investigating shrinkage changes of natural pozzolan based geopolymer cement paste. Iranian Journal of Material Science. 2011. 8(3). Pp. 50–60.

20. Wallah, S.E. Drying shrinkage of heat-cured fly ash-based geopolymer concrete, World applied Science. 2009. 3(12). Pp. 12–21.

21. Kim, J.K., Lee C.-S. Prediction of differential drying shrinkage in concrete. Cement and Concrete Research. 1998. 28(7). Pp. 985–994

22. Slowik, V., Ju, J.W. Discrete modeling of plastic cement paste subjected to drying, in: e.a.e. B. H. Oh (Ed.) Fracture Mechanics of Concrete and Concrete Structures-Recent Advances in Fracture Mechanics of Concrete Korea Concrete Institute, 2010. Pp. 1–6.

23. Tam, C.M., Tam, V.W.Y., Ng, K.M. Assessing drying shrinkage and water permeability of reactive powder concrete produced in Hong Kong. Construction and Building Materials. 2012. 26(1). Pp. 79–89.

24. Tangchirapat, W., Jaturapitakkul, C. Strength, drying shrinkage, and water permeability of concrete incorporating ground palm oil fuel ash. Cement and Concrete Composites. 2010. 32(10). Pp. 767–774.

25. ASTM C150 / C150M-16e1, Standard Specification for Portland Cement, ASTM International, West Conshohocken, PA, 2016, www.astm.org

26. Yusuf, M.O., Megat, Johari, Ahmad, M.A., Arifin, Z.A., Maslehuddin M. Effects of addition of Al(OH)3 on the strength of alkaline activated ground blast furnace slag-ultrafine palm oil fuel ash (AAGU) based binder. Construction and Building Materials. 2014. 50 (0). Pp. 361–367.

27. Yusuf, M.O., Megat, Johari, Ahmad, M.A., Arifin, Z.A., Maslehuddin M. Effects of H2O/Na2O molar ratio on the Strength of Alkaline Activated Ground Blast Furnace Slag-Ultrafine Palm Oil Fuel Ash Based Concrete. Materials & Design. 2014. 56(0). Pp. 158–164.

28. ASTM C-1437, Standard Test Method for Flow of Hydraulic Cement Mortar, American Society for Testing and Materials, ASTM International, West Conshohocken, PA, www.astm.org, 2013.

29. ASTM C-33, Standard specification for concrete aggregate, American Society for Testing and Materials, ASTM International, West Conshohocken, PA, www.astm.org, 2001.

30. Yusuf, M.O., Megat Johari, M.A., Ahmad, Z.A., Maslehuddin, M. Shrinkage and strength of alkaline activated ground steel slag/ultrafine palm oil fuel ash pastes and mortars. Materials & Design. 2014. 63. Pp. 710–718.

31. Scherer, G.W. Aging and drying of gels. Journal of Non-Crystalline Solids. 1988. 100. Pp. 77–92.

32. Adamson, A.W., Gast, A.P. Physical Chemistry of Surfaces, 6th Ed., Wiley-Interscience. New York, 1997.

33. Collins, F.G., Sanjayan, J.G. Workability and mechanical properties of alkali activated slag concrete. Cement and Concrete Research. 1999. 29. Pp 455–458.

34. Sagoe-Crenstil, K., Brown, T., Taylor A. Drying shrinkage and creep performance of geopolymer concrete. Journal of Sustainable Cement- A. Based Materials. 2013. 2(1). Pp. 35–42.

Contacts:

Moruf Yusuf, +966598373550; moruf@uhb.edu.sa